



HAL
open science

A large-eddy simulation model for pesticide dispersal during spray application

Ali Chahine, Sylvain Dupont, Yves Brunet, Carole Sinfort

► **To cite this version:**

Ali Chahine, Sylvain Dupont, Yves Brunet, Carole Sinfort. A large-eddy simulation model for pesticide dispersal during spray application. Conférence Internationale sur les écotechnologies pour l'agriculture en Europe AgEng 2010, Labo/service de l'auteur, Ville service, Pays service., Sep 2010, Clermont-Ferrand, France. hal-02757084

HAL Id: hal-02757084

<https://hal.inrae.fr/hal-02757084>

Submitted on 3 Jun 2020

HAL is a multi-disciplinary open access archive for the deposit and dissemination of scientific research documents, whether they are published or not. The documents may come from teaching and research institutions in France or abroad, or from public or private research centers.

L'archive ouverte pluridisciplinaire **HAL**, est destinée au dépôt et à la diffusion de documents scientifiques de niveau recherche, publiés ou non, émanant des établissements d'enseignement et de recherche français ou étrangers, des laboratoires publics ou privés.

A large-eddy simulation model for pesticide dispersal during spray application

A. Chahine^{1,2}, S. Dupont¹, Y. Brunet¹, C. Sinfort²

¹ INRA, UR1263 EPHYSE, 71 avenue Edouard Bourleaux, F-33140 Villenave d'Ornon, France

² UMR ITAP, Cemagref, BP 5095, 34033 Montpellier Cedex, France

Email: ali.chahine@bordeaux.inra.fr

Abstract

Evaluating pesticide loss and the resulting air concentration requires experimental data and numerical modelling. In the present study the wind flow within a vineyard canopy has been characterized using the Large-Eddy Simulation (LES) method for solving turbulent flow. A Lagrangian approach was also used to track the trajectory of the droplets emitted by an air-assisted sprayer. In parallel, field experiments were performed to characterize and evaluate upward pesticide loss, as well as investigate the wind generated by the sprayer and its effect on the droplet plume emitted in the plot. Some first results are provided along these lines. It is further shown how the dispersal of a pesticide plume during a spray treatment can be simulated with the coupled LES-Lagrangian approach. The first model outputs provide information on the wind field characteristics in a vineyard and on the instantaneous and time-averaged patterns of pesticide dispersal from a moving sprayer. Keywords: Pesticide, LES, Lagrangian model, Turbulent dispersion.

1. Introduction

Atmospheric pollution by pesticides is a major social concern as it constitutes a potential source for public health deficiency (Nagayama et al., 2007; Elbaz et al., 2009). High pesticide concentration in the air observed in the vicinity of agricultural areas results essentially from droplet drift during spray applications and the evaporation of droplets that have not deposited on the ground or the vegetation (Bedos et al., 2002).

It is acknowledged that the amount of pesticide subject to far field dispersion depends upon many factors. Wind speed, ambient temperature and atmospheric stability are the main meteorological parameters that influence the fate of the droplet plume during spray application (Gil et al., 2007). Several studies also focussed on other factors such as the sprayer type and the diameter of emitted droplets (Ozkan et al., 1995; Wood et al., 2001). During spray application over dense enough vegetation a large amount of droplets deposit on the plant elements. However very dense vegetation canopies may deviate upwards the droplet plume brought by the air stream from the air-assisted sprayer, resulting in a relatively small droplet deposition flux and a large loss into the atmosphere (Raupach & Leys, 1999).

The present study focusses on pesticide dispersal over a vineyard during spray application. For this purpose, an experiment was firstly performed over an artificial vineyard in order to quantify and understand pesticide dispersal and the main wind flow characteristics, as modified by the sprayer. Then a new airflow model coupled with a dispersal model was developed using large-eddy simulation and Lagrangian approaches, respectively, in order to track individual droplet trajectories and determine the air concentration field at the plot scale. The LES approach has the advantage of simulating instantaneous dynamical wind fields, thereby reproducing wind gusts in the vine plot. It is therefore well suited to be coupled with a Lagrangian dispersal model.

The main characteristics of the experiment and models are presented in section 2. In section 3 we present and discuss some of our experimental results on pesticide dispersal, and we then show a first example of application of the model over an infinite vineyard.

2. Material and methods

Experiment

The experiment on pesticide drift was undertaken in the Cemagref research centre at Montpellier in June 2009, using the methodology of Gil et al. (2007). The plot consisted of four artificial vine rows of 1.5 m height and 10 m length. The thickness of each row was 0.40 m and the inter-row was 2 m (Fig. 1a). The experiment consisted in quantifying pesticide ground deposition and aerial dispersal, as well as characterizing wind flow during the passage of the sprayer.

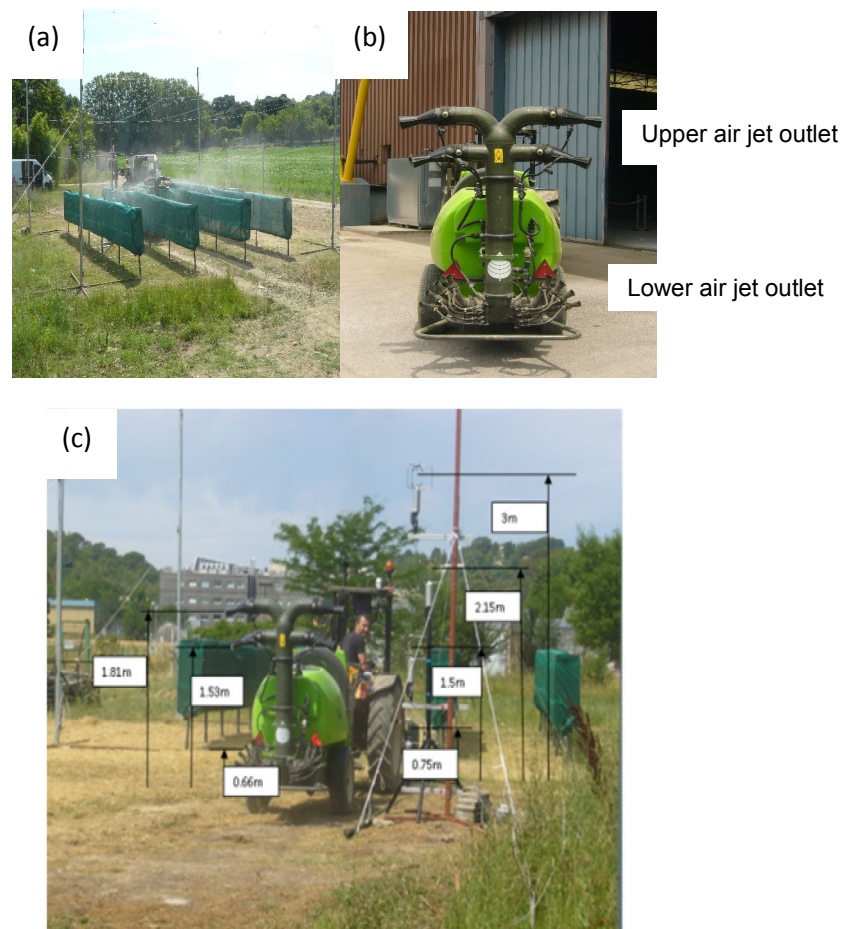


Fig. 1: (a) The experimental plot with four artificial rows, (b) the Tecnomas Pulsar sprayer, (c) the sonic anemometer mast used in static tests.

The same spray liquid as in Gil et al. (2007) was used in place of a true pesticide solution. In order to measure ground deposition, band collectors were placed on the ground between rows. To assess pesticide loss above the artificial canopy, three horizontal planes of PVC line collectors were set at three heights: 2.8 m, 4 m and 5.7 m. The amount of spray deposited on the line collector planes allows the amount of pesticide drifting out of the plot to be assessed. The sprayer used in the experiment was a Tecnomas Pulsar air-assisted

orchard sprayer shown in Fig. 1b. The spray application was made from the central row with a sprayer forward speed of 1.52 m s^{-1} and a spray flow rate of 0.14 l s^{-1} . The deposition on band and line collectors was analysed a few minutes after the spray application by using the same procedure as in Gil et al. (2007).

The main characteristics of the wind flow induced by the sprayer air jets were deduced from three sonic anemometers mounted at 0.75, 1.5 and 3 m on a mast located in the central row. Outside from the plot, another sonic anemometer was located at a height of 3 m to record the ambient meteorological conditions. Furthermore, the magnitude of the wind generated by the sprayer air jets was assessed in a static configuration where the sprayer was placed behind a mast equipped with four sonic anemometers and located outside the plot, as shown in Fig. 1c.

Model

The airflow model is based on the large-eddy simulation method. The equations of motion are spatially filtered with a filter of the same size as the mesh size in the grid domain. Thus only the large eddies are solved while the small eddies are modelled using a turbulence model based on the resolution of a subgrid scale turbulent kinetic energy equation. The momentum equation writes:

$$\bar{\rho} \left(\frac{\partial \tilde{u}_i}{\partial t} + \tilde{u}_j \frac{\partial \tilde{u}_i}{\partial x_j} \right) = - \frac{\partial}{\partial x_i} \left(\bar{p}' - \alpha_{div} \frac{\partial \bar{\rho} \tilde{u}_j}{\partial x_j} \right) - \frac{\partial \tau_{ij}}{\partial x_j} - \bar{\rho} C_d A_f \sqrt{\tilde{u}_j \tilde{u}_j} \tilde{u}_i, \quad (1)$$

where the overtilde indicates the filtered variables. In equation (1), $\bar{\rho}$ is the base state density of the air (kg m^{-3}), p is the air pressure, t is time and x_i ($x_1=x$, $x_2=y$, $x_3=z$) are the streamwise, lateral and vertical directions, respectively; u_i ($u_1=u$, $u_2=v$, $u_3=w$) are the instantaneous velocity components along x_i , α_{div} is a damping coefficient used to attenuate the acoustic waves. The variables C_d and A_f are the drag force coefficient and the frontal area density of the vegetation ($\text{m}^2 \text{ m}^{-3}$), respectively. These two parameters account for the effect of vegetation on the wind flow according to the drag force approach.

The subgrid stress tensor τ_{ij} is modelled through a subgrid scale eddy viscosity as follows,

$$\tau_{ij} = -\bar{\rho} \nu_t \left(\frac{\partial \tilde{u}_i}{\partial x_j} + \frac{\partial \tilde{u}_j}{\partial x_i} \right), \quad (2)$$

where ν_t is the eddy viscosity modelled as a function of the length and velocity scales characterizing the subgrid scale eddies: $\nu_t = 0.1 \sqrt{e} l$.

The length scale l is the grid spacing $l = (\Delta x \Delta y \Delta z)^{1/3}$, where Δx , Δy and Δz are the grid size components in the streamwise, lateral and vertical directions, respectively. The subgrid scale velocity is obtained by solving the conservation equation of the turbulent kinetic energy e contained in the small unsolved eddies:

$$\frac{\partial e}{\partial t} + \tilde{u}_j \frac{\partial e}{\partial x_j} = -\tau_{ij} \frac{\partial \tilde{u}_i}{\partial x_j} - \frac{g}{\theta} \tau_{3\theta} + \frac{\partial}{\partial x_j} \left(2\nu_t \frac{\partial e}{\partial x_j} \right) - C_\varepsilon \frac{e^{3/2}}{l} - 2C_d A_f \sqrt{\tilde{u}_j \tilde{u}_j} e. \quad (3)$$

The terms on the right hand side of equation (3) represent, respectively, the shear production, the buoyancy production, the turbulent transport, the dissipation and the cascade term for subgrid scale turbulent kinetic energy (see Dupont and Brunet, 2008).

In the Lagrangian dispersal model, a pesticide droplet emitted from the sprayer into the atmosphere experiences the drag force that the ambient air exerts on its surface and the gravity force due to its apparent weight. Assuming that there is no interaction between droplets and neglecting subgrid scale dispersal, the motion of each droplet is described by the Newton's second law (see for example Teske et al., 2002):

$$\frac{d\bar{x}_p(t)}{dt} = \bar{v}_p(t) \quad (4a)$$

$$\frac{d\bar{v}_p(t)}{dt} = \frac{\bar{v}(\bar{x}_p(t), t) - v_p(t)}{\tau_p} q(Re_p) + \bar{g}, \quad (4b)$$

where \bar{v}_p is the velocity of a droplet, $\bar{v}(\bar{x}_p(t), t)$ is the air velocity at the droplet position $\bar{x}_p(t)$ determined following equation (1), \bar{g} is the acceleration of gravity. The droplet inertia is characterized by the relaxation time τ_p given by $\tau_p = \rho_p d_p^2 / 18\rho\nu$, where d_p and ρ_p are the diameter and density of droplets, respectively, and ν is the molecular air kinematic viscosity.

The particle Reynolds number is given as $Re_p = |\bar{v}_p - \bar{v}| d_p / \nu$ and $q(Re_p)$ is a function of particle Reynolds number (Re_p) that takes into account the non-linear effect of the drag force as follows (Clift et al., 1978):

$$\begin{aligned} q(Re_p) &= 1 \text{ if } Re_p < 1, \\ q(Re_p) &= 1 + 0.15 Re_p^{0.687} \text{ if } Re_p \geq 1. \end{aligned} \quad (5)$$

This Lagrangian dispersal model is based on that developed by Vinkovic et al. (2006) for solid particles. In this first application of the model to pesticide droplets, volatilization of droplets after emission was not considered.

Numerical setup

A numerical simulation of pesticide dispersal was performed over a vineyard represented by a periodic distribution of vegetated rows. Each vine row had a width of 0.6 m and the inter-row was 2 m wide. Thus when the wind blows over the canopy, it experiences a resistance at the position of the rows and no resistance in the gap. The resistance in the row is proportional to the drag coefficient C_d ($C_d = 0.2$) and the frontal area density A_f , (see equation 1). Fig. 2 shows a vertical cross section of the vine rows in the computational domain, with an in-row leaf area index of about 5.

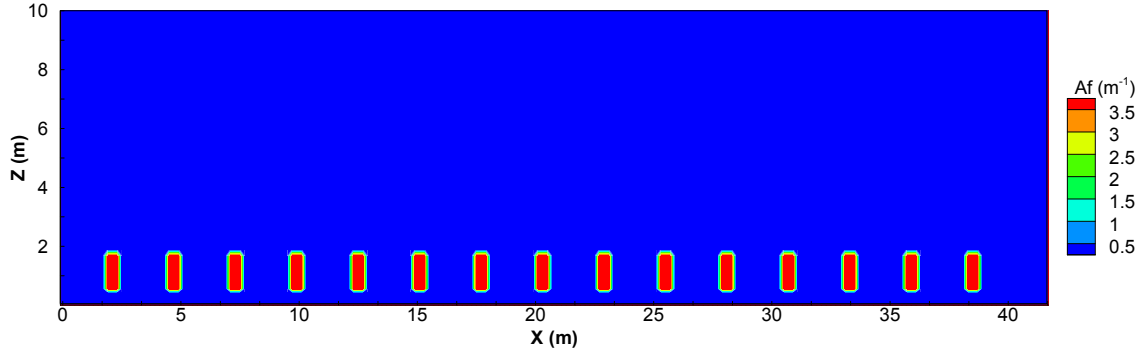


Fig. 2: Representation of the simulated vine canopy in a vertical cross section. The colours represent the frontal area density A_f .

The computational domain is $41 \times 10 \times 24 \text{ m}^3$ with a horizontal spatial resolution of 0.2 m and a mesh stretched in the z-direction so that 10 layers are present within the canopy. The boundary conditions of the domain are periodic in the x and y-directions; the canopy can thus be considered as infinite. At the top boundary a Rayleigh damping layer 6 m thick is used in order to absorb the upward-propagating wave and eliminate wave reflection at the top of the domain. The wind blows from the left to the right boundaries, i.e. the wind is perpendicular to the vine rows. The velocity field is initialized in the domain by a meteorological pre-processor (Pénelon et al., 2001). After the wind has adjusted with the canopy, the wind field is averaged along the y-direction and over 100 instantaneous wind field realizations.

Once dynamic equilibrium is reached, droplets are emitted in one row by considering a Gaussian distribution with a mean diameter of $100 \mu\text{m}$ and a variance of $10 \mu\text{m}$, and with an initial velocity of 10 m s^{-1} . The source is defined as a virtual vertical rectangular band located along the row; its height is equal to the diameter of the output sprayer and its length to that of the vine row. Droplets are assumed to deposit on the ground when they reach the height of 0.1 m. Their deposition on the vegetation elements are described by two processes: impaction with plant elements and sedimentation on the horizontal projection of the plant elements (Chamberlain, 1967; Ferrandino & Aylor, 1985).

3. Results and discussion

Experimental results

Fig. 3 shows the correlations between the experimental relative upward loss against the air temperature T and the standard deviation of the vertical wind velocity component σ_w . We observe a significant correlation between the upward loss and both variables with a high confidence coefficient R , showing an increase in the upward loss with increasing temperature and vertical velocity variance. A smaller correlation ($R = 0.14$) is obtained between the upward loss and the intensity of turbulence, defined as the square root of the half-sum of the three velocity component variances. In our experimental conditions the vertical wind velocity standard variation σ_w therefore appears as the most representative turbulent parameter responsible for upward loss. The horizontal wind velocity variances may be increased by fluctuations in wind direction without significant variations in vertical velocity and upward loss.

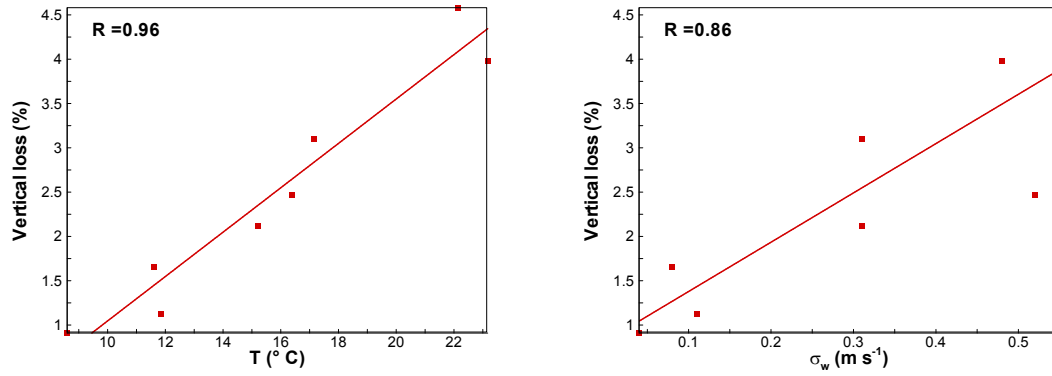


Fig. 3: Correlations between upward loss and meteorological parameters (left: air temperature, right: standard deviation of the vertical velocity). Regression lines from experimental points are indicated.

Fig. 4 shows horizontal profiles of pesticide ground deposition inside and outside the plot for eight experiments. Deposition is quantified as the fraction of spray deposited per unit area. In all experiment the deposition curves present similar shapes. This is due to the fact that the wind speed is sufficiently low compared to the air jet velocity, so that the droplets deposit in the same way in all experiments. Inside the plot ($-4 \text{ m} \leq x \leq 4 \text{ m}$) all deposition curves present a minimum at the position of the driving sprayer ($x = 0$) and a maximum on each lateral side, followed by a strong decrease. Outside the plot ($|x| > 4 \text{ m}$) the deposition curves continue to decrease asymptotically.

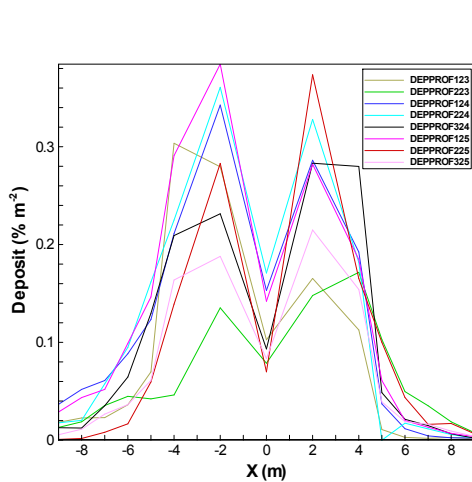


Fig. 4: Ground deposition along x .

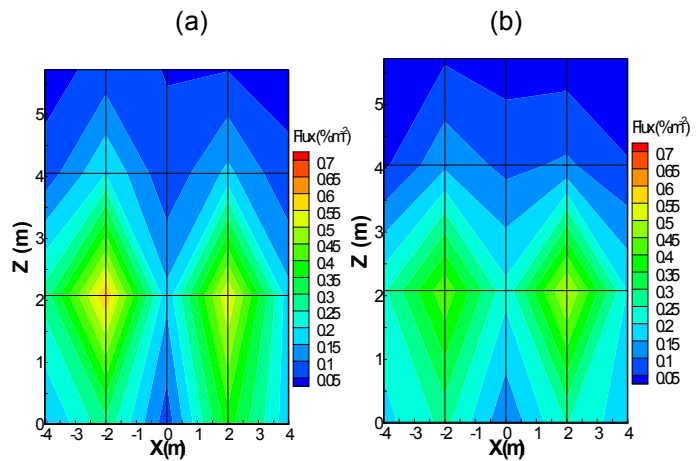


Fig. 5: Spatial structure of the flux for one of the experiment (a) and over all experiments (b).

The analysis of deposition on the line collectors set up in three horizontal planes shows that its variation in the x -direction follows the same spatial pattern as ground deposition. In order to characterize the spatial correlation between ground and aerial deposition we computed the time-integrated flux at the position of each collector. For band collectors this flux represents ground deposition while for line collectors above the canopy it represents the upward loss. Fig. 5 illustrates the spatial structure of the flux for one experiment and the spatial structure averaged over all experiments. Each node of the grid corresponds to the location of a collector. At $z = 0$, the nodes correspond to the ground band collectors. From these spatial structures, it appears that deposition on the band collectors is lower than that on line collectors which is maximum at $z = 2.8 \text{ m}$. This result means that upward fluxes are larger

than downward fluxes. The presence of two maxima at $x = -2$ and 2 m is explained by the air jets of the sprayer.

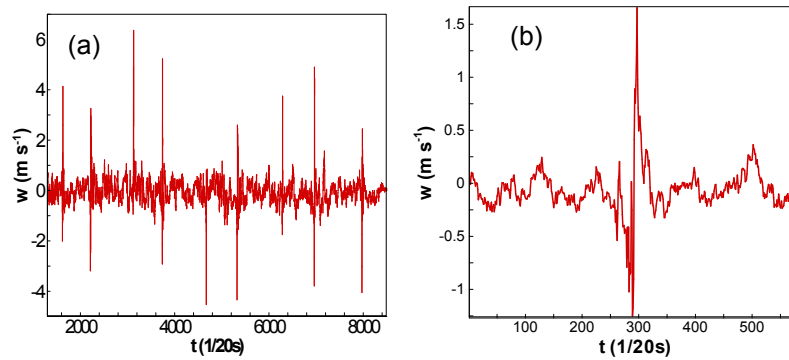


Fig. 6: (a) Vertical wind velocity w signal recorded by the anemometer located at $z = 1.5$ m during 10 passages of the sprayer, (b) averaged w signal over 10 passages.

Fig. 6a shows the vertical velocity w recorded by the anemometer closest to the upper air jet output located at $z = 1.5$ m during 10 passages of the sprayer. On this figure, we notice 10 pairs of positive and negative peaks, with the negative ones always preceding the positive ones. Fig. 6b shows the average pattern of w during the passage of the sprayer. The positive peak is caused by the lower upward air jet of the sprayer, as shown from the w signals recorded during the static tests by the anemometer located at $z = 1.5$ m (Fig. 1c); w is always positive with an estimated initial velocity of the order of 24 m s^{-1} using formulas of jet theory (Klein, 2003). Two factors may be responsible for the negative peak: (i) the upper air jet of the sprayer is slightly oriented downwards, with a small angle toward the sonic located at $z = 1.5$ m, and (ii) the aspiration of the lower turbine located at the front of the sprayer, before the air jets. The analysis of the time shift between positive and negative peaks shows that it corresponds to the horizontal separation distance between the upper and lower air jets, so that the origin of the negative peak is probably related to the upper air jets. Hence the maximum of pesticide flux in the spatial structure (Fig. 5) may be explained by the orientation of the lower jets that emit pesticide droplets toward the position of the lowest aerial collectors. This feature can be relatively well observed in Fig. 7.



Fig. 7: Illustration of the upward direction of the lower jet of the sprayer.

First application of the model

In order to illustrate the model behaviour over an infinite vineyard, Fig. 8 shows the main characteristics of the wind within and above the vine canopy when the wind blows perpendicularly to the vine rows (from left to right).

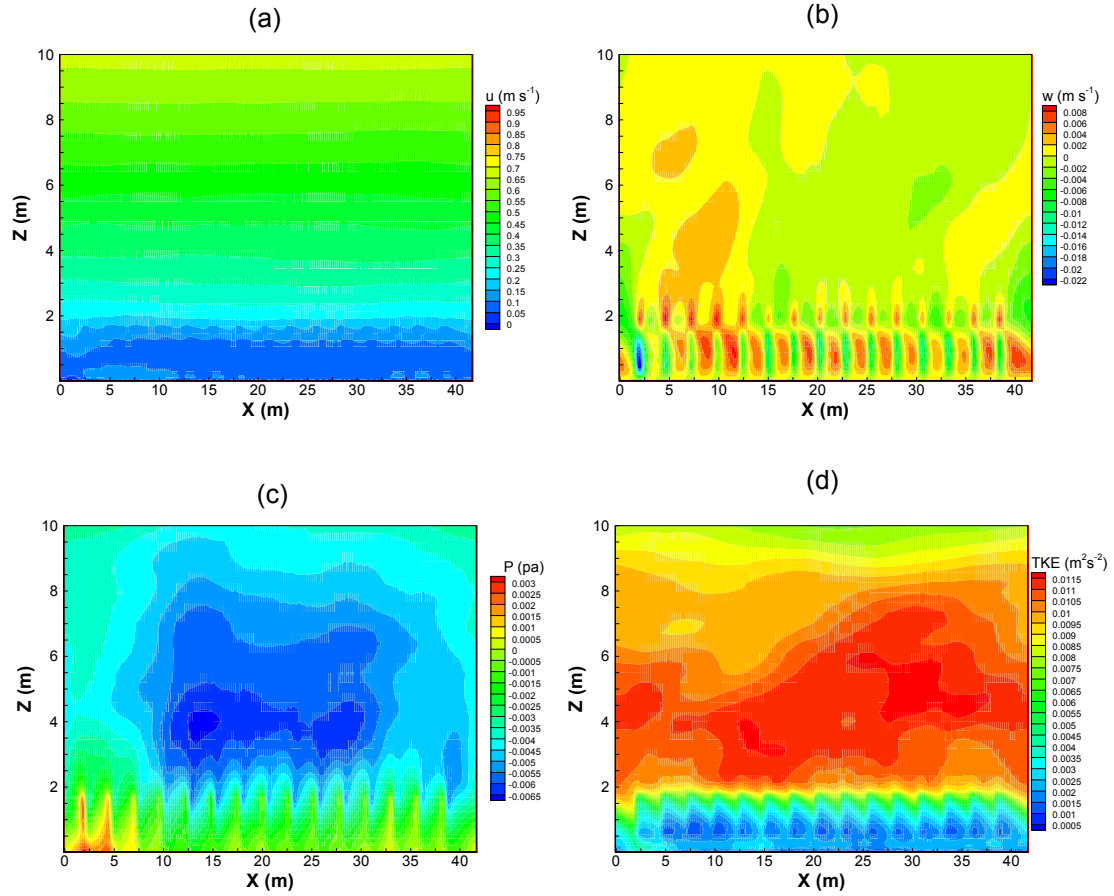


Fig. 8: Mean wind field characteristics: (a) streamwise velocity u , (b) vertical velocity w , (c) pressure perturbations P and (d) turbulent kinetic energy TKE over a 1.7 m height vineyard.

For all wind variables, we clearly observe the effect of the vine rows on the mean fields. The mean streamwise velocity u decelerates within the canopy due to the aerodynamic resistance of the vine rows (Fig. 8a). In the canopy the mean vertical velocity w is slightly positive in the gaps and negative within the rows (Fig. 8b); the opposite occurs just above the canopy, indicating the presence of small vortices. The effect of the vegetation on the pressure field is also visible in Fig. 8c. The turbulent kinetic energy in the canopy (Fig. 8d) is smaller in the rows due to an increase in turbulence dissipation, whereas between the rows it slightly increases as a consequence of wake development behind the rows.

Regarding droplet dispersion, Fig. 9a-b shows a snapshot of the plume emitted from the moving sprayer located at height $z = 1.7$ m, and Fig. 9c presents the mean droplet concentration field near the source, as time-averaged over 50 plume realizations. It can be clearly seen that upward dispersion and horizontal transport of droplets are significant for the finest ones (blue-colored droplets in the same figure) while the heavier droplets deposit more rapidly near the source.

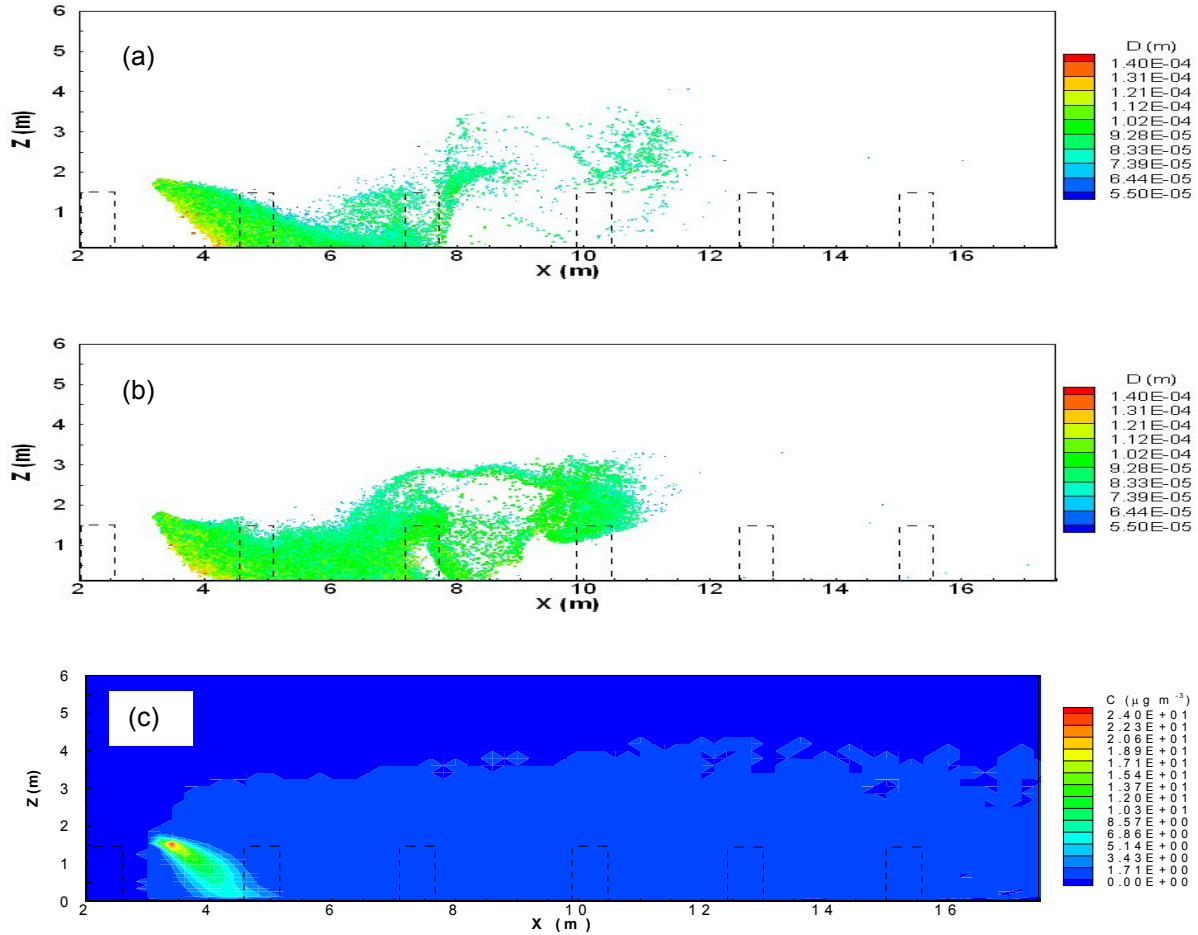


Fig. 9: (a) Droplet plume at $t = 900$ s and (b) $t = 950$ s, (c) average droplet concentration field. The dashed rectangles represent the position of the rows.

4. Conclusion

In this study we demonstrated the possibility of investigating pesticide dispersal over a vineyard canopy from in-situ experiments and a coupled LES-Lagrangian approach. The next steps will consist in (i) introducing a better representation of the sprayer air jets in the model, (ii) validating the simulated wind flow over a vineyard against an in-situ experiment planned in summer 2010 and (iii) validating simulated droplet dispersal against the experiment presented in this study. In the future, the model could be applied in more complex vineyard configurations and further provide guidelines to reduce atmospheric pesticide dispersal.

Acknowledgments

We would like to thank the Montpellier Cemagref team for their help with the experimental protocol and data analysis. We also thank Didier Garrigou and Dr. Mark R. Irvine for their help with the experimental part of the work. Computer simulations related to this work were performed on the Ephyse cluster. Thanks are expressed to Patrick Moreau, Tovo Rabemanantsoa, Guy Pracros and Dr. Mark R. Irvine for their help with the cluster set-up.

References

- Bedos, C., Cellier, P., Calvet, R. & Barriuso, E. (2002). Occurrence of pesticides in the atmosphere in France. *Agronomie*, 22, 35-49.
- Chamberlain, A.C. (1967). Transport of *Lycopodium* spores and other small particles to rough surfaces. *Proc. Roy. Soc. London A296*, 45-70.
- Clift, R., Grace, J. R. & Weber, M. E. (1978). *Bubbles, drops and particles* Academic Press, Academic press.
- Dupont, S. & Brunet, Y. (2008). Influence of foliar density profile on canopy flow: a large-eddy simulation study. *Agric. For. Meteorol.* 148, 976-990.
- Elbaz, A., Clavel, J., Rathouz, P. J., Moisan, F., Galanaud, J. P., Delemotte, B., Alperovitch, A. & Tzourio, C. (2009). Professional Exposure to Pesticides and Parkinson Disease. *Annals Of Neurology*, 66, 494-504.
- Ferrandino, F. J. & Aylor, D. E. (1985). An explicit equation for deposition velocity. *Boundary-Layer Meteorol.* 31,197-201.
- Gil, Y., Sinfort, C., Guillaume, S., Brunet, Y., Polveche, V. & Bernard, B. (2007). Atmospheric loss of pesticides above an artificial vineyard during air-assisted spraying. *Atmospheric Environment* 41, 2945-2957.
- Klein, M., Sadiki, A. & Janicka, J. (2003). A digital filter based generation of inflow data for spatially developing direct numerical or large eddy simulations. *Journal of Computational Physics*, 186, 652-665.
- Nagayama, J., Tsuji, H., Iida, T., Nakagawa, R., Matsueda, T., Hirakawa, H., Yanagawa, T., Fukushima, J. & Watanabe, T. (2007). Immunologic effects of perinatal exposure to dioxins, PCBs and organochlorine pesticides in Japanese infants. *Chemosphere*, 67, 393-398.
- Ozkan, H. E., Reichard, D. L., Zhu, H. & Babeir, A. S. (1995). Drift retardant chemical effects on spray droplet size, pattern and drift. *Agri. Sci.*, 7, 2, 131-140.
- Pénelon, T., Calmet, I. & Mironov, DV. (2001). Micrometeorological simulations over a complex terrain with SUBMESO: a model study using a novel pre-processor. *Int. J. Environ. Pollut.*, 16, 583-602.
- Raupach, M. R. & Leys, J. F. (1999). The efficacy of vegetation in limiting spray drift and dust movement, *Tech. Rep. 47. CSIRO land and water, Canberra, Australia.*
- Teske, M. E., Bird, S. L., Esterly, D. M., Curbishley, T. B., Ray, S. L. & Perry, S. G. (2002). AgDRIFT: A model for estimating near-field spray drift from aerial application. *Environmental Toxicology and Chemistry*, 213, 659-671.
- Thistle, H. W., Teske, M. E. & Reardon, R. C. (1998). Weather effects on drift meteorological factors and spray drift: An overview. *Proceedings of the North American Conference on Pesticide Spray Drift Management.*
- Vinkovic, I., Aguirre, C., Ayrault, M. & Simoëns, S. (2006). Large-eddy simulation of the dispersion of solid particles in a turbulent boundary flow. *Boundary-layer Meteorology*, 121, 283-311.
- Woods, N., Craig, I. P., Dorr, G. & Young, B. (2001). Spray Drift of Pesticides Arising from Aerial Application in Cotton. *Environ. Qual.*, 30, 697-701.